

# SAR SHIP DETECTION FOR ROUGH SEA CONDITIONS

Pasquale Iervolino<sup>(a)</sup>, Raffaella Guida<sup>(a)</sup>, Donato Amitrano<sup>(a)</sup> and Armando Marino<sup>(b)</sup>

<sup>(a)</sup>Surrey Space Centre, University of Surrey, Guildford, United Kingdom  
{p.iervolino, r.guida}@surrey.ac.uk

<sup>(b)</sup>University of Stirling, Biological and Environmental Sciences, Stirling, United Kingdom  
armando.marino@stir.ac.uk

## ABSTRACT

In the Synthetic Aperture Radar (SAR) framework many detection algorithms and techniques have been published in the recent literature; however the detection of vessels whose dimensions are in the order of the image spatial resolution is still challenging in rough sea state scenarios. This issue is addressed in the paper presented here by comparing rationale and performance of two detectors developed by the same authors: the Generalized Likelihood Ratio Test (GLRT) and the Intensity Dual-Polarization Ratio Anomaly Detector (iDPolRAD). Both detectors are tested on a dual-polarization VV/VH Interferometric Wide Swath Sentinel-1 image acquired over the Suruga Bay on the Pacific Coast of Japan. The theory is presented here and the two detectors are compared against the Cell Average-Constant False Alarm Algorithm (CA-CFAR) showing both better performance than CFAR in terms of false alarms rejection.

**Index Terms**— SAR, Maritime Surveillance, ship detection, Generalized Likelihood Ratio Test (GLRT), polarimetry.

## 1. INTRODUCTION

The request for maritime security and safety applications has increased in the recent past. In this scenario, Synthetic Aperture Radar (SAR) sensors are one of the most effective means thanks to their capability to get images independently from daylight and weather conditions. SAR sensors are considered a valid alternative to the traditional coastal-based surveillance systems (such as the Automatic Identification System) and are particularly suitable for the detection and the tracking of ships and vessels in open sea.

In the SAR ship-detection field, many algorithms have been presented in literature for single and multi-polarization channels [1-3]. Traditionally, SAR ship-detection algorithms rely on Constant False Alarm Rate (CFAR) methods in which the sea clutter is modelled according to a distribution function and a threshold is then computed to achieve a desired probability of false alarm [1]. All the clusters of

pixels with intensity greater than the set threshold are considered as potential ships. As a consequence, detectors are strongly influenced by thresholding techniques applied to the SAR amplitude or intensity image with two main negative results in the performance: 1) a high false alarm rate and 2) the inability to detect ships with Radar Cross Section (RCS) values in the order of the RCS of the surrounding sea clutter.

The main objective of this paper is to compare (in terms of performance and computational load) two detectors developed by the authors themselves: the Generalized Likelihood Ratio Test (GLRT) [4, 5] and the Intensity Dual-Polarization Ratio Anomaly Detector (iDPolRAD) [6, 7]. It has been already proved that these ship detectors overperform traditional CFAR algorithms [5-7]. Here, the GLRT and the iDPolRAD are employed to monitor maritime areas subject to particular harsh weather conditions (worst case scenario for ship detection algorithms) by using Sentinel-1 images with single and dual polarization. The paper is organized as follows: in section 2 the rationale behind the new detectors is introduced; in section 3 the case study is presented; in section 4 some results are shown and in section 5 conclusive remarks and future perspective are briefly commented.

## 2. SAR SHIP DETECTORS

The novel methodologies which will be applied to the case study are introduced in the following sub-sections.

### 2.1 Generalized Likelihood Ratio Test

The GLRT is a model-based approach and sets a statistical test based on the ratio of the likelihood functions relative to the ship (target, hypothesis  $H_1$ ) and the sea background (clutter, hypothesis  $H_0$ ). In particular, the distribution function of the sea background can be computed as performed for CFAR algorithms. It has been demonstrated that the clutter function is *Gamma* distributed in the intensity domain for homogenous clutter while it is *K* distributed in

inhomogeneous background with a spiky speckle texture [8]. On the other side, the distribution function of the target is derived from electromagnetic models within Geometric Optic (GO) and Kirchhoff Approximation (KA). Within these hypotheses, it has been proved that the target is *Gamma* distributed in the co-polarized (HH and VV) channels and *Weibull* distributed in the cross-polarized (HV and VH) channels at S-, C- and X- bands [9]. At this point, when both the clutter and the target distributions are defined, the GLRT can be set according to the following equation:

$$\Lambda_G(\sigma_x) = \frac{p(\sigma_x/H_1, \hat{\alpha}_t)}{p(\sigma_x/H_0, \hat{\alpha}_c)} \sigma_{pq}^0 > T(PFA) \leftrightarrow \text{Detected} \quad (1)$$

where  $\Lambda_G(\cdot)$  is the generalized likelihood ratio function,  $\hat{\alpha}_t$  and  $\hat{\alpha}_c$  are the Maximum Likelihood Methods (MLE) estimators relative to the target (hypothesis  $H_1$ ) and the clutter (hypothesis  $H_0$ ) distribution parameters respectively;  $\sigma_{pq}^0$  is the backscattering coefficient at polarization  $pq$  (with  $p$  and  $q$  standing for horizontal H, or vertical V polarization) and  $T(PFA)$  is the threshold given a fixed probability of false alarm, respectively.

As for the CFAR algorithms, the GLRT can be applied by using a moving window and computing the clutter and target parameters along with the threshold at each iteration (Adaptive Threshold algorithm); or, viceversa, the target and clutter parameters can be estimated through the MLE for a single representative window yielding to a fix threshold (Global Threshold algorithm) [10].

## 2.2 Intensity Dual-Polarization Ratio Anomaly Detector

The iDPolRAD is a dual-polarization detector and was initially developed for iceberg detection [6]. It exploits the different scattering properties between the sea clutter and the ship target: targets produce an increase of either volume scattering or multiple reflections compared to the surrounding sea areas and the iDPolRAD is able to detect anomalies of the previous two scattering mechanisms [5, 6]. In order to implement the detector, two boxcar filters are applied over the VH and VV intensity image: a smaller test window  $w_{test}$  and a larger training window  $w_{train}$ . The detector can be written as follows:

$$I = \frac{\langle |VH|^2 \rangle_{test} - \langle |VH|^2 \rangle_{train}}{\langle |VV|^2 \rangle_{train}} \sigma_{HV}^0 = \Lambda \sigma_{HV}^0 > T_A \quad (2)$$

where  $\langle \rangle_{test}$  and  $\langle \rangle_{train}$  are the spatial average using the test and the training windows respectively and  $T_A$  is the test threshold. Details about the test and training windows are

provided in [6].  $\Lambda$  term of equation (2) can be rewritten after some mathematical manipulations as follows [6]:

$$\Lambda = \rho_{ring} \frac{1+c}{R\rho^{-1} + cRVH^{-1}} - \rho_{train} \quad (3)$$

where  $\rho$  is the cross-over co-polarization ratio and is defined as depolarization ratio. The subscript is used to define if this estimation is performed in the *training* area or in the *ring* (the region between the test and the training window) area.  $R\rho$ ,  $RVH$  and  $c$  are defined by the following equations:

$$\begin{aligned} R\rho &= \frac{\rho_{test}}{\rho_{ring}} \\ RVH &= \frac{\langle |VH|^2 \rangle_{test}}{\langle |VV|^2 \rangle_{ring}} \\ c &= \frac{N_{train}}{N_{test}} \end{aligned} \quad (4)$$

where  $N_{train}$  and  $N_{test}$  are the number of pixels inside the training and the test window, respectively.

It has been proved in [6] that: a)  $\Lambda \rightarrow 0$  if the depolarization ratio and the cross-polarized intensity (VH) do not change between the ring and the test area (i.e. sea clutter and all homogeneous areas); b)  $\Lambda \rightarrow \infty$  if the depolarization ratio and the VH intensity sharply increase between the ring and the test area (i.e. ship target enter the test window) c)  $\Lambda \rightarrow -\rho_{train}$  if the volume and multiple reflections decrease from the ring to the test area (i.e. a pool of open water in multi-year sea ice).

Summarizing, when a target (ships, vessels) is in the test window, the  $\Lambda$  value drastically increases and a detection is triggered.

Both detectors are tested over a meaningful case study as explained in the next section.

## 3. CASE STUDY

The algorithms are tested on SAR images acquired by the European Sentinel-1 constellation. At this aim, multiple Interferometric Wide Swath Ground Range Detected (IWS-GRD) products have been selected over the coast of Japan. For the sake of brevity one dataset is presented in this abstract, while multiple products will be included in the final version of the paper. The SAR images were acquired between September and December 2018 in rough sea conditions. In fig.1 (a)-(b) the intensity of the crop (1600x1600 pixels) relative to the input image acquired on 29<sup>th</sup> September 2018 at VV and VH polarization is shown, respectively. In Table I the main acquisition parameters are reported for this SAR acquisition.

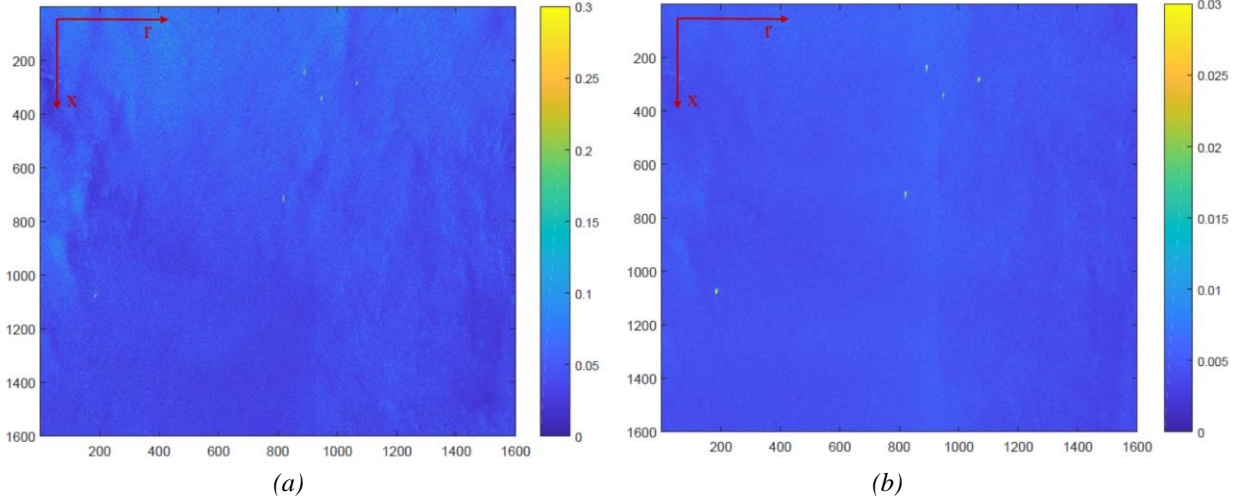


Fig. 1: False color SAR intensity image acquired by the Sentinel-1 constellation on 29<sup>th</sup> September 2018 over Suruga Bay in azimuth ( $x$ )/slant range  $\otimes$  plane at HH (a) and HV polarization (b).

TABLE I: SAR ACQUISITION PARAMETERS

| Parameter                   | Value            |
|-----------------------------|------------------|
| Acquisition Date            | 29 September     |
| Acquisition Mode            | IWS              |
| Data Type                   | GRD              |
| Azimuth Resolution [m]      | 22               |
| Ground Range Resolution [m] | 20               |
| Azimuth pixel spacing [m]   | 10               |
| Ground Range pixel spacing  | 10               |
| Orbit                       | Descending Right |
| Radar look angle [deg]      | 30°              |
| Working frequency [GHz]     | 5.4              |
| Polarization                | VV/VH            |

#### 4. RESULTS

First of all, a land masking is performed by using the Shuttle Radar Topography Mission (SRTM) 1 arc-second data (approximately 30 m spatial resolution) and the SNAP software developed by the European Space Agency (ESA). Then, images are radiometrically calibrated to obtain the backscattering coefficient (images in *sigma nought* domain) and multilooked (3x3) in order to reduce the speckle noise and obtain a square pixel (30m) in both azimuth and ground range directions.

After these pre-processing steps, the clutter and targets statistics are computed over moving windows to retrieve the statistical vectors ( $\hat{a}_t$  and  $\hat{a}_c$ ) and implement the GLRT.

Similarly, the statistics over the training and the target windows are computed for the VV and VH channels to implement the iDPolRAD. In particular, the boxcar filters have been chosen of 41x41 pixels and 49x49 pixels for the test and training window, respectively.

Finally, regarding the CA-CFAR, an Adaptive Threshold algorithm is chosen with a clutter *Gamma* distributed while

the probability of false alarm is set to  $10^{-6}$ . The detection maps relative to the CA-CFAR, the GLRT and the iDPolRAD are shown in Fig. 2 where the green rectangles represent true targets and the red rectangles the false alarms. It is clear that both GLRT and iDPolRAD overperform the CFAR being able to reject almost all the false alarms without missing any genuine targets. Detection and false alarm rates are reported in Table II for all the detectors considered in this paper where the ground truth data are based on a visual inspection analysis performed by the authors themselves.

In order to better compare the detection and the false alarm probabilities, the Receiver Operating Characteristic (ROC) curves are computed for the GLRT, CFAR and iDPolRAD at C-band and by considering ten IWS products at C-band with a VV+VH dual polarization configuration. At this aim, more than 200 ships are manually selected on the SAR images by the authors and each ship is considered as a detection if at least one pixel is above the detector's threshold. ROC curves are shown in Fig. 3 in blue, red and green for the GLRT, CFAR and iDPolRAD, respectively and are consistent with the detection map of Fig. 2: best performance are obtained for the iDPolRAD and the second best for the GLRT. This is partially explained by the greater target-to-clutter ratio (2dB on average) at VH polarization than VV polarization.

#### 5. CONCLUSIONS

Two recent ship detection algorithms (GLRT and iDPolRAD) for SAR imagery have been presented and compared against the CA-CFAR algorithm. The GLRT is a model-based detector and relies on a single polarization product, while the iDPolRAD does not rely on any electromagnetic model simulation but it needs the intensity.

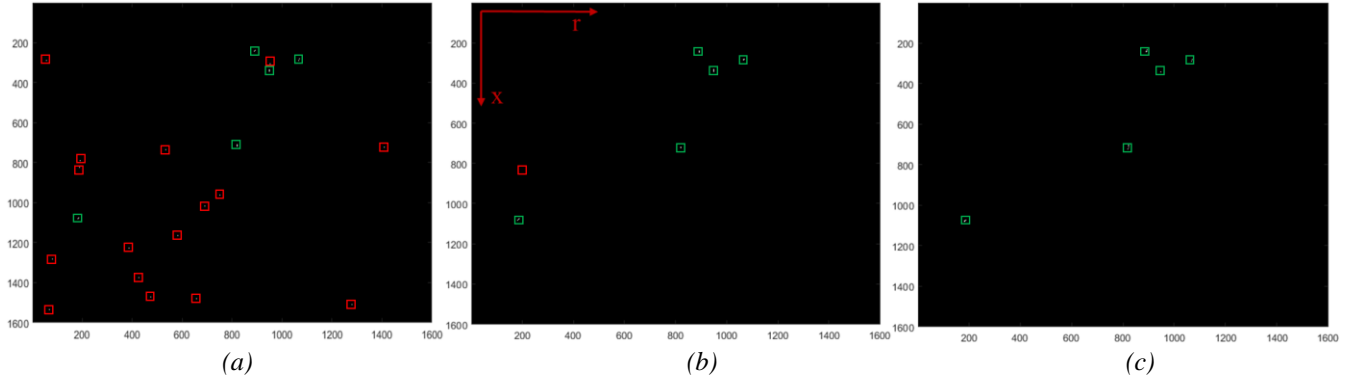


Fig. 2: Detection maps in azimuth ( $x$ )/slant range ( $r$ ) plane where the green rectangles represents true targets and the red rectangles false alarms: CA-CFAR (a), GLRT (b) and iDPolRAD (c).

TABLE II: CFAR, GLRT AND DPOLRAD OUTCOMES

|          | False Alarms | Detected Targets | Missing Targets |
|----------|--------------|------------------|-----------------|
| CFAR     | 16           | 5                | 0               |
| GLRT     | 1            | 5                | 0               |
| iDPolRAD | 0            | 5                | 0               |

(or the amplitude) of the co- and cross-polarized channels to be processed

Results show much better performance for both the detectors than *classical* CFAR algorithm with the probability of detection 1% higher at a fixed probability of false alarm of  $10^{-5}$ . In future, detection maps will be validated with additional data (i.e. terrestrial and satellite AIS) while GLRT and iDPolRAD compared against different sea states and working frequencies (S- and X-band).

## 6. REFERENCES

[1] D.J.Crisp, "The State-of-Art in Ship Detection in Synthetic Aperture Radar Imagery", DSTO Information Science Laboratory, 2004.

[2] Y. Cui, J. Yang, Y. Yamaguchi, G. Singh, S. Park, and H. Kobayashi, "On semiparametric clutter estimation for ship detection in synthetic aperture radar images," *IEEE Trans. Geosci. Remote Sens.*, vol. 51, no. 5, pp. 3170–3180, May 2013.

[3] X. Leng, K. Ji, K. Yang, and H. Zou, "A bilateral CFAR algorithm for ship detection in SAR images," *IEEE Geosci. Remote Sens. Lett.*, vol. 12, no. 7, pp. 1536–1540, Jul. 2015.

[4] P. Iervolino, R. Guida, and P. Whittaker, "A novel ship-detection technique for Sentinel-1 SAR data", *Proc. APSAR*, Singapore, Sep. 2015, pp. 797-801.

[5] P. Iervolino and R. Guida, "A Novel Ship Detector Based on the Generalized-Likelihood Ratio Test for SAR Imagery," *IEEE J. Sel. Topics Appl. Earth Observ. Remote Sens.*, vol. 10, no. 8, pp. 3616-3630, Aug. 2017.

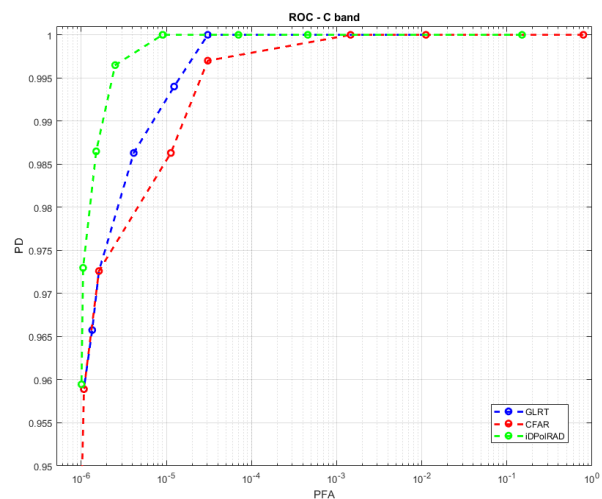


Fig. 3: ROC curves relative to the GLRT (blue), CFAR (red) and iDPolRAD (green) at C-band.

[6] A. Marino, W. Dierking and C. Wesche, "A Depolarization Ratio Anomaly Detector to Identify Icebergs in Sea Ice Using Dual-Polarization SAR Images," in *IEEE Transactions on Geoscience and Remote Sensing*, vol. 54, no. 9, pp. 5602-5615, Sept. 2016.

[7] A. Marino and P. Iervolino, "Ship detection with Cosmo-SkyMed PINGPONG data using the dual-pol ratio anomaly detector," *Proc. IGARSS*, Fort Worth, TX, Jul. 2017, pp. 3897-3900.

[8] J. Lee and E. Pottier, *Polarimetric Radar Imaging: From Basics to Applications*. Boca Raton, FL, USA: CRC Press, Taylor & Francis, 2009.

[9] P. Iervolino, R. Guida, and P. Whittaker, "A model for the backscattering from a canonical ship in SAR imagery", *IEEE J. Sel. Topics Appl. Earth Observ. Remote Sens.*, vol. 9, no. 3, pp. 1163–1175, March 2016.

[10] P. Iervolino et al., "Ship detection in SAR imagery: A comparison study," *Proc. IGARSS*, Fort Worth, TX, Jul. 2017, pp. 2050-2053.